Preparation and Characterization of Ag Doped Mn_2O_3 Nanomaterial for CO Oxidation

R. K. Kunkalekar and A. V. Salker*

Department of Chemistry, Goa University, Goa 403206 India

Abstract: Nano-sized silver doped Mn_2O_3 was synthesized by starch assisted co-precipitation technique. The prepared samples were tested for CO oxidation reaction. Ag doped Mn_2O_3 sample was found to show higher activity then pristine Mn_2O_3. XRD patterns authenticate the formation of Mn_2O_3 phase. Electron microscopy images show that the particles are in nano-sized, agglomerated and 40 - 70 nm in range. Thermal analysis data indicates the phase change from Mn_2O_3 to Mn_3O_4 beyond 950 ^oC. Magnetic susceptibility data indicates the paramagnetic nature of these samples. Electrical resistivity measurement shows that these samples are semiconductors.

Keywords: Mn_2O_3, Ag doped Mn_2O_3, Co-precipitation, Electron microscopy, Thermal analysis, Carbon monoxide oxidation.

1. INTRODUCTION

Among the transition metal oxides, manganese oxides are of special interest because of their varied oxidation states as exemplified by MnO, MnO_2, Mn_2O_3, Mn_3O_4, Mn_2O_7 etc. and which is found to be greatly dependent on the preparation conditions. Manganese oxides are non-toxic, cost effective and have a wide range of technical applications, viz. catalysis for completely oxidizing various volatile organic substances, molecular adsorption, ion exchange, biosensor, high density magnetic storage media, electrochemical super capacitor and promising cathode material for lithium batteries [1-4] due to their outstanding structural flexibility and physical properties.

One such important functional metal oxide is Mn_2O_3, which has captured the interest of many researchers owing to its wide applications [5-7]. Its higher surface area is especially of great significance for catalytic applications. Mn_2O_3 with different structural features have been extensively investigated as an inexpensive, environmental friendly catalyst to remove waste gases. When combined with noble metals, it shows a higher catalytic activity at a relatively lower temperature [8-10].

Over the years, the oxidation of CO to CO_2 has remained the major solution towards CO abatement in air depollution treatments. The development of catalytic converters has led to an extraordinary high number of publications on metal oxide catalysts during the last several years. The appropriate combination of manganese oxides and some mixed metal oxides exhibit greater activity and thermal stability for this reaction than the single metal oxides [11]. Better results were achieved by using a combination of noble metals with transition metal oxides which led to a higher catalytic activity at a relatively lower temperature for the CO oxidation reaction along with good stability [12-13]. Mn_2O_3 in combination with noble metal either doped or supported are widely used for low temperature CO oxidation reactions [8-10]. Nanostructured materials have been actively studied as a catalyst material by many researchers due to the various advantages offered as a result of size reduction. Various techniques have been employed to prepare nano-sized Mn_2O_3 with different morphologies such as nano-arrays, nano-wires, nano-spheres, and clusters [14-16] which greatly influences their catalytic activity for CO oxidation reaction.

In the present investigations, the synthesis of nano-sized Ag doped Mn_2O_3 using starch is being reported for the first time. The prepared samples were characterized by different instrumental techniques. The prepared samples have been tested for CO oxidation reaction and the results obtained are noteworthy.

2. EXPERIMENTAL

2.1. Catalysts Preparation

Nano-sized Mn_2O_3 and $Mn_{1.95}Ag_{0.05}O_3$ catalysts were prepared by starch assisted co-precipitation method [17]. Calculated amount of AR grade manganese acetate and silver nitrate were dissolved in distilled water. Both these solutions were added to 2% starch solution at 100 ^oC with stirring. Liquid ammonia was added drop wise with continuous stirring to achieve a pH = 9. Subsequently, the suspension was subjected to oxidation by drop wise addition of 30% H_2O_2 solution with constant stirring in order to adjust the oxidation state of metal ions. The suspension was then stirred continuously at 100 ^oC till dryness. The resulting product was dried at 150 ^oC for 6 h. Finally, the dried precipitate was homogenized by grinding using a mortar and pestle and calcined in air at 700 ^oC for 5 h.

2.2. Catalysts Characterization

The phase composition of the calcined samples was analyzed by X-ray diffraction (XRD) using RIGAKU Ultima IV diffractometer using Cu *Kα* radiation (λ = 1.5418 Å) with 2θ scanning range 10–80^o. Phase identification was made using the standard XRD reference database. The surface morphol-

*Address correspondence to this author at the Department of Chemistry, Goa University, Goa 403206 India; Tel: +92-832-6519315;
Fax: +91-832-2452889; E-mail: sal_arun@rediffmail.com

2211-5455/13 $58.00+.00

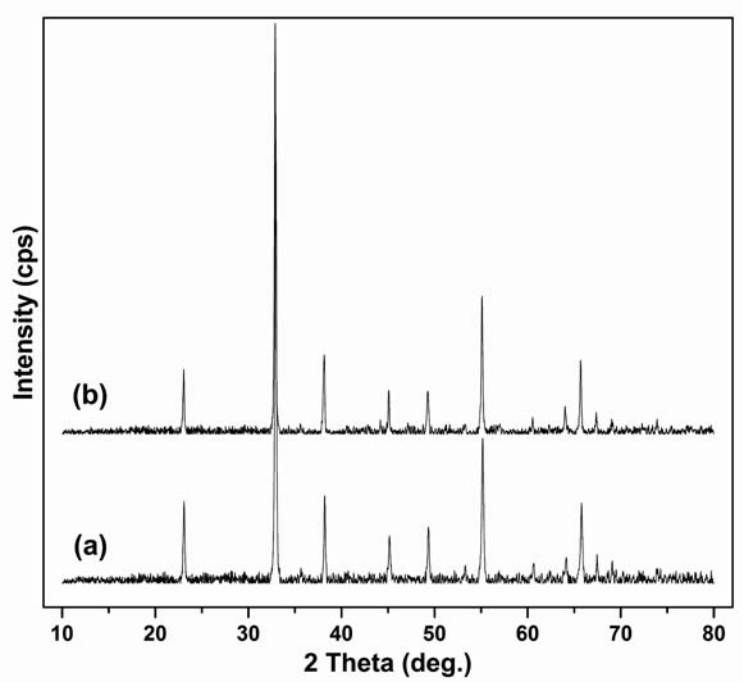

Fig. (1). XRD patterns of (**a**)Mn_2O_3 and (**b**) $Mn_{1.95}Ag_{0.05}O_3$.

ogy was determined with JSM-5800LV scanning electron microscope (SEM) instrument operating at 20 kV. Transmission electron microscopy (TEM) images were taken on a PHILIPS CM 200 electron microscope operating with an accelerating voltage of 200 KV. The BET surface area was measured by nitrogen adsorption at liquid Nitrogen temperature using a SMART SORB–91 surface area analyzer. The samples were regenerated at 200 °C for 2 h prior to the adsorption experiments. Thermal analysis were carried out on a NETZCH STA 409 PC TG/DSC instrument in air at a heating rate of 10 °C min^{-1} and heated from ambient to 1100 °C. Fourier transform infra-red (FTIR) analysis of the samples were undertaken in the range 400-1500 cm^{-1} with SHIMADZU IR prestige-21 spectrophotometer. Temperature variation of electrical resistivity from room temperature to 400 ^oC was measured in a conductivity unit cell by two probe method in air. Samples in the form of pellet of 0.75 cm radius and 0.15 cm thickness were used. Pellets were heated at 150 °C for 2 h in oven prior to measurements. Magnetic susceptibility of the samples were measured using the Guoy's balance at room temperature in a field of 8600 gauss and using $Hg[Co(SCN)_4]$ as the standard material. Magnetic susceptibility (χ_g) and magnetic moment (μ_{eff}) values were then determined accordingly.

2.3. Catalytic Activity Test

The catalytic tests for CO oxidation by O_2 were performed at atmospheric pressure in a continuous flow, fixed bed glass reactor. The sample powder of 0.9 g was supported between glass wool plugs in a glass reactor which was placed in an electric furnace. The reaction temperature was measured by inserting a thermo-couple in the middle of the catalyst bed. The catalytic activity was determined using a feed gas composition of 5% CO and 5% O_2 in nitrogen. All these three gases were first mixed in a mixing bulb. The individual gas flow rates were controlled using flow meters and precision needle valves, previously calibrated for each specific gas. Prior to the CO oxidation reaction the catalyst was activated by passing O_2 at 100 °C for 30 min. The mixture of gases was then allowed to pass over the catalyst at a rate of 5000 ml h^{-1}. The feed gases and the products were analyzed employing an online Gas Chromatograph with molecular sieve 13X and Porapak Q columns, H_2 was used as a carrier gas. The CO was prepared in the laboratory by standard procedure and further purified by passing through alkali and molecular sieve traps. O_2, N_2 and H_2 gases were used from pure commercial cylinders.

3. RESULTS AND DISCUSSION

3.1. Characteristic Properties

Fig. (**1a** and **b**) shows X-Ray diffraction pattern for pristine Mn_2O_3 and doped $Mn_{1.95}Ag_{0.05}O_3$ samples. The Fig. (**1a**) shows the characteristic diffraction features which can be indexed to the cubic system of Mn_2O_3 being consistent with the reported values for Mn_2O_3 (ICDD card No: 01-1061). From this diffraction pattern, it is evident that the product has high crystallinity owing to the well defined sharp peaks. The $Mn_{1.95}Ag_{0.05}O_3$ (Fig. **1b**) shows almost similar diffraction features as that of Mn_2O_3. No extra reflections can be seen for Ag which indicates well incorporation of Ag into the Mn_2O_3 lattice.

The morphology and particle size is illustrated using the SEM images for the pure Mn_2O_3 and doped $Mn_{1.95}Ag_{0.05}O_3$ samples. The pristine Mn_2O_3 (Fig. **2a**) shows almost spherical morphology and particles are agglomerated in appearance. The particles were in the range of 40 – 70 nm in diameter. The $Mn_{1.95}Ag_{0.05}O_3$ shows morphology (Fig. **2b**) similar to that of pristine Mn_2O_3. The particles were found to be spherical in shape and agglomerated in appearance to some extent. The average particle size is approximately 80

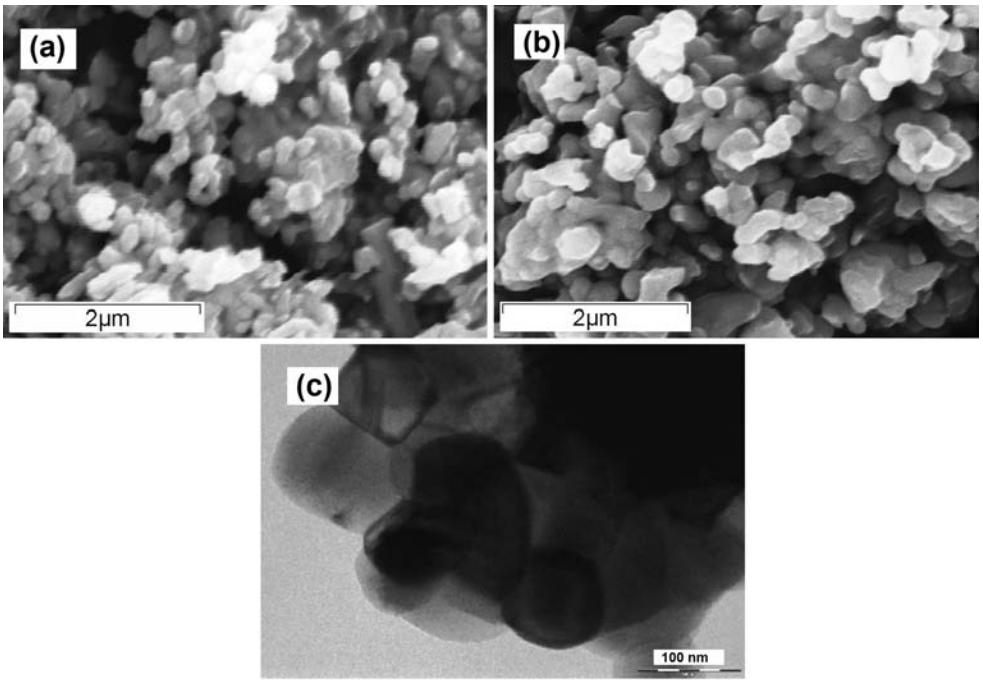

Fig. (2). SEM images of (**a**) Mn_2O_3, (**b**) $Mn_{1.95}Ag_{0.05}O_3$ and TEM image of (**c**) $Mn_{1.95}Ag_{0.05}O_3$.

Table 1. Shows BET Surface Area, Gram Susceptibility (X_g), Magnetic Moment (μ_{eff}) Values and Catalytic Activity of 50% (T_{50}) and 100% (T_{100}) CO Conversion

Sample	SA (m^2g^{-1})	X_g	μ_{eff} (B.M.)	T_{50} (^oC)	T_{100} (^oC)
Mn_2O_3	6.6	$6.8204x10^{-5}$	5.1278	210	310
$Mn_{1.95}Ag_{0.05}O_3$	1.7	$6.6912x10^{-5}$	5.0380	188	240

nm. These observations are attributed to the preparation method which is known to influence the morphology and particle size of the materials.

Furthermore, TEM analysis was employed to examine the particle nature and particle size of this catalyst. TEM image of $Mn_{1.95}Ag_{0.05}O_3$ is shown in Fig. (**2c**). From TEM image it is clear that the particles are nano-sized and almost spherical in shape. The particle size was found to be in range of 40 - 70 nm.

The specific BET surface area of the calcined samples has been determined using nitrogen physisorption at liquid nitrogen temperature. The results are summarized in Table **1**. These samples exhibits lower surface area mainly due to higher calcination temperature and agglomeration of particles as observed in SEM/TEM images. The undoped Mn_2O_3 shows a surface area of 6.6 m^2g^{-1}. After incorporation of Ag in Mn_2O_3 lattice, the surface area decreases.

Thermal study of Mn_2O_3 shows the major weight loss in 950-1050 ^oC region (Fig. **3a**) with a corresponding endothermic peak in DTA curve, this weight loss is due to the loss of oxygen and transformation of the phase from Mn_2O_3 to Mn_3O_4 [18]. The $Mn_{1.95}Ag_{0.05}O_3$ sample also shows similar weight loss pattern with an endothermic peak as can be seen in Fig. (**3b**). However, a little shift in the phase transformation temperature is observed in case of the $Mn_{1.95}Ag_{0.05}O_3$ sample, which shows a phase transformation at a slightly higher temperature. This may be one of the consequences of Ag incorporation into the Mn_2O_3 lattice [19, 20]. From the TG/DTA investigations, it is confirmed that the phase form is Mn_2O_3 phase since no apparent weight loss was observed for MnO_2 to Mn_2O_3 phase transformation which otherwise is usually seen above 530 ^oC [20,21]. This data also confirms that after calcining the samples at 700 °C, formation of Mn_2O_3 phase takes place.

The samples were also characterized by FTIR in the region of 1500–400 cm^{-1}. Fig. (**4**) shows the FTIR spectra of (**a**) Mn_2O_3 and (**b**) $Mn_{1.95}Ag_{0.05}O_3$. The Mn_2O_3 (Fig. **4a**) shows several vibrational modes at 673, 608, 574, 530, 453 cm^{-1} which are characteristic of Mn_2O_3 oxide [22]. The bands at ~673 and 574 cm^{-1} [23] are attributed to Mn–O stretching vibrations of Mn_2O_3 and the one at 530 cm^{-1} is due to Mn–O bending vibrations of Mn_2O_3. All the vibrations are also prominent in $Mn_{1.95}Ag_{0.05}O_3$ sample indicating that the crystal structure of Mn_2O_3 is retained even after doping. These bands are found to be shifted in frequency to some extent which may be due to the effect of Ag doping in the lattice structure of Mn_2O_3.

In order to investigate the temperature dependent conductivity, the samples were subjected to resistivity measurements from room temperature to 400 ^oC in static air. Fig. (**5**) shows the plot of electrical resistivity verses temperature in the temperature range from ambient to 400 ^oC. The dc

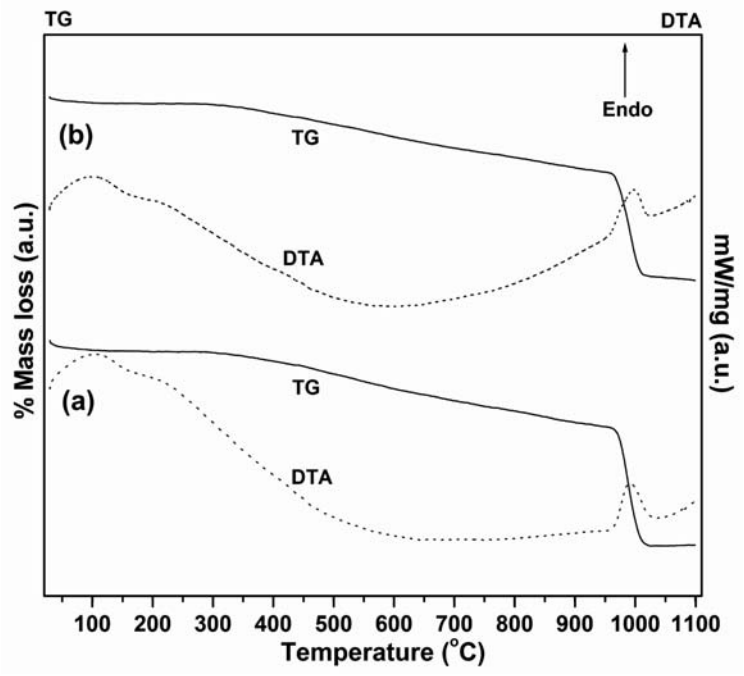

Fig. (3). Thermal analysis (TG/DTA) patterns of (**a**) Mn_2O_3 and (**b**) $Mn_{1.95}Ag_{0.05}O_3$.

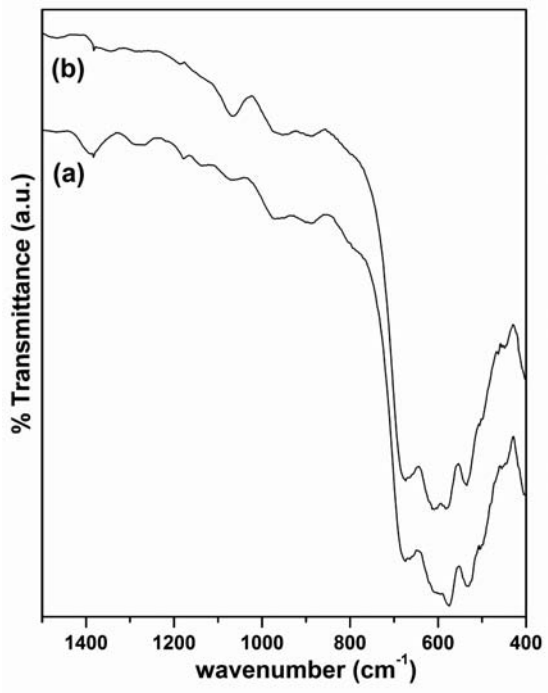

Fig. (4). FTIR spectra of (**a**) Mn_2O_3 and (**b**) $Mn_{1.95}Ag_{0.05}O_3$.

electrical conductivity is found to be strongly dependent on temperature. It can be seen that conductance of both the pure Mn_2O_3 and Ag doped Mn_2O_3 increases with increasing temperature and exhibits semiconductor behavior. Fig. (**5**) shows that at lower temperature conductivity of both the samples have almost similar slopes, i.e. the same activation energies at the lower temperature range. However, at higher temperature conductivity increases remarkably and falls in Arrhenius region. Ag doped sample is found to be slightly more conducting than the pristine sample. At lower temperature the low conductivity values are concluded as extrinsic, whereas at higher temperature linear increase in conductivity is observed and is called as an intrinsic semiconductivity. In order to check the reproducibility of conductivity data as a function of temperature the samples were run several times and the same trend is observed as that which has been reported here.

The magnetic susceptibility of the oxide samples was determined by using the Guoy's balance at room temperature, using field strength of 8600 gauss. The observed gram sus-

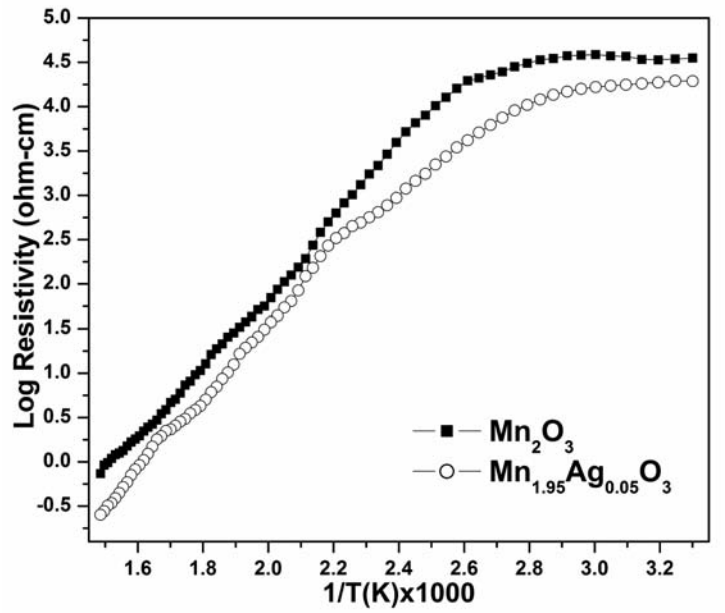

Fig. (5). Temperature variation of electrical resistivity from room temperature to 400 °C.

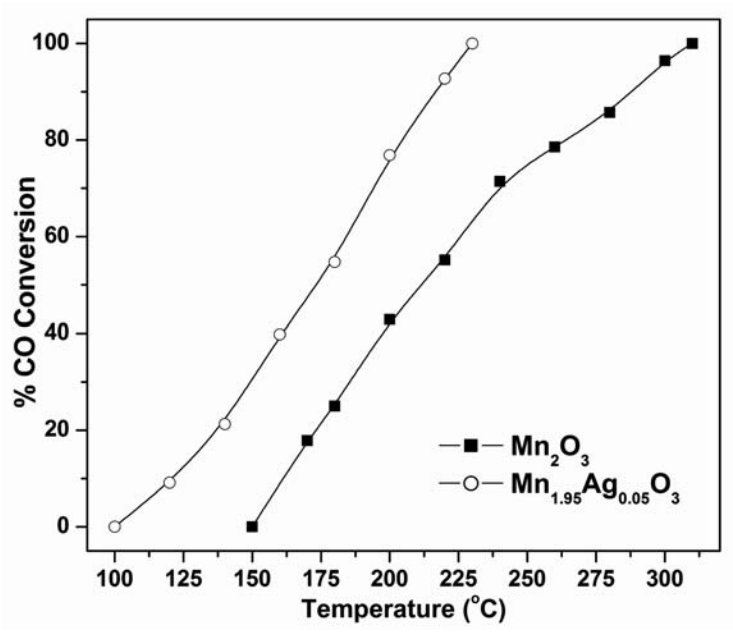

Fig. (6). Catalytic performances of catalysts towards CO oxidation. (Conditions : 5% CO, 5% O_2 in N_2 at rate of 5000 ml h^{-1}).

ceptibility values and magnetic moment values at room temperature are presented in Table **1**. The magnetic moment values were found to be ~ 5.1 B.M. for the samples. These values confirm that manganese is present in 3+ oxidation state having four unpaired electrons in Mn_2O_3 oxide. The pristine Mn_2O_3 showed higher values of magnetic susceptibility and magnetic moment values than the doped $Mn_{1.95}Ag_{0.05}O_3$ sample. With incorporation of Ag these values were found to be decreasing due to the influence of Ag ions in Mn_2O_3 lattice.

3.2. Catalytic Activity

The catalytic activity of the prepared samples was tested for CO oxidation reaction. Fig. (**6**) illustrates the catalytic activity of the samples. The Ag doped Mn_2O_3 catalyst showed good activity as compared to pristine Mn_2O_3. The Mn_2O_3 showed complete conversion of CO at a temperature of 310 °C whereas the Ag doped catalyst show the conversion at 230 ^oC, which is around 80 ^oC lower than pristine Mn_2O_3. In Table **1** the light–off temperatures of 50% CO conversion (T_{50}) and 100% CO conversion (T_{100}) over different samples are presented. Introduction of Ag in Mn_2O_3 greatly improved the catalytic behavior of Mn_2O_3, a drastic decrease in total CO conversion temperature was also observed. The BET surface area of silver doped Mn_2O_3 was found to be very less as can be seen in Table **1**. Interestingly, despite having a lower surface area this catalyst showed good activity. Undoubtedly, the higher activity is due to the presence of the Ag species.

Generally CO oxidation on manganese oxides follows a mechanism proposed by Mars - Van Krevelen [24] implying that lattice oxygen incorporation occurs during CO oxidation and that the reduced surface of the manganese oxide is rejuvenated by taking up oxygen from the feed mixture. CO is adsorbed on the surface as bi-dentate carbonate, the adsorbed CO extracts surface oxygen atom to form CO_2 and surface oxygen vacancy. The oxygen vacancy is filled by gas phase O_2, weakening the bond in O_2 molecule. This adsorbed O_2 species, which is believed to be present possibly as O_2^- ion radical, may react readily with a neighboring CO molecule adsorbed as a bidentate carbonate, forming CO_2 again and recovering back the catalysts surface. Presence of Ag greatly improved this activity by increasing the active sites.

4. CONCLUSIONS

Starch assisted co-precipitation method was employed for the synthesis of nano-sized $Mn_{1.95}Ag_{0.05}O_3$. The XRD diffraction pattern confirmed the formation of Mn_2O_3 phase. The nano-sized nature of the particles was determined by electron microscopy. Thermal analysis gave significant evidence of phase change of Mn_2O_3 to Mn_3O_4 at around 950 - 1050 ^oC. FTIR spectroscopy data gives characteristic Mn-O vibrations typical of Mn_2O_3. Electrical resistivity data proves the semiconducting nature of these samples. Magnetic susceptibility measurements revealed the presence of 4 unpaired electrons in the oxide samples. Despite having a lower surface area, the Ag doped Mn_2O_3 was found to markedly improve the catalytic activity for CO oxidation reaction as compared to the pristine Mn_2O_3. These results unambiguously prove the ability of noble metals in enhancing the catalytic properties of simple oxides.

CONFLICT OF INTEREST

The authors confirm that this article content has no conflicts of interest.

ACKNOWLEDGEMENTS

The authors are grateful to University Grant Commission, New Delhi, for the financial support under research project.

REFERENCES

[1] Kumar, R.; Sithambaram, S.; Suib, S.L. Cyclohexane oxidation catalyzed by manganese oxide octahedral molecular sieves-Effect of acidity of the catalyst. *J. Catal*., **2009**, *262*, 304–313.

[2] Cao, J.; Zhu, Y.; Shi, L.; Zhu, L.; Bao, K.; Liu, S.; Qian, Y. Double-shelled Mn_2O_3 hollow spheres and their Application in water treatment. *Eur. J. Inorg. Chem.*, **2010**, *8*, 1172–1176.

[3] Xue, X.Y.; Xing, L.L.; Wang, Y.G.; Wang, T.H. Preparation, characterization and electrical transport properties of individual α-MnO_2 and β-MnO_2 nanorods. *Solid State Sci.*, **2009**, *11*, 2106–2110.

[4] Chandra, S.; Das, P.; Bag, S.; Bhar, R.; Pramanik, P. Mn_2O_3 decorated graphene nanosheet: An advanced material for the photocatalytic degradation of organic dyes. *Mater. Sci. Engg. B*, **2012**, *177*, 855– 861.

[5] Jin, M.; Kim, J.W.; Kim, J.M.; Jurng, J.; Bae, G.N.; Jeon, J.K.; Park, Y.K. Effect of calcination temperature on the oxidation of benzene with ozone at low temperature over mesoporous α-Mn_2O_3. *Powder Technol*., **2011**, *214*, 458-462.

[6] Ramírez, A.; Friedrich, D.; Kunst, M.; Fiechter, S. Charge carrier kinetics in MnO_x, Mn_2O_3 and Mn_3O_4 films for water oxidation. *Chem. Phys. Lett*., **2013**, *568-569*, 157-160.

[7] Cao, F.; Li, H.; Xu, Z.; Zhang, J.; Zhang, Y.; Huo, Y. Preparation of Mn_2O_3/SBA-15 catalyst with high loading and catalytic peroxidation for degradation of organic pollutants. *J. Mol. Catal. A: Chem.*, **2012**, *353-354*, 215-219.

[8] Imamura, S.; Tsuji, Y.; Miyake, Y.; Ito, T. Cooperative action of palladium and Manganese (III) oxide in the oxidation of carbon monoxide. *J. Catal*., **1995**, *151*, 279–284.

[9] Wang, L.C.; Huang, X.S.; Liu, Q.; Liu, Y.M.; Cao, Y.; He, H.Y.; Fan, K.N.; Zhuang, J.H. Gold nanoparticles deposited on manganese(III) oxide as novel efficient catalyst for low temperature CO oxidation. *J. Catal*., **2008**, *259*, 66–74.

[10] Kunkalekar, R.K.; Salker, A.V. Activity of Pd doped and supported Mn_2O_3 nanomaterials for CO oxidation. *Reac. Kinet. Mech. Cat*., **2012**, *106*, 395–405.

[11] Abdel Halim, K.S.; Ismail, A.M.; Khedr, M.H.; Abadir, M.F. Catalytic Oxidation of CO Gas over Nanocrystallite $Cu_x Mn_{1-x} Fe_2O_4$. *Top. Catal*., **2008**, *47*, 66–72.

[12] Zou, Z.Q.; Meng, M.; Zha, Y.Q. Surfactant-Assisted Synthesis, Characterizations, and catalytic oxidation mechanisms of the mesoporous MnOx−CeO_2 and Pd/MnOx−CeO_2 catalysts used for CO and C_3H_8 oxidation. *J. Phys. Chem. C*, **2010**, *114*, 468–477.

[13] Salker, A.V.; Kunkalekar, R.K. Palladium doped manganese dioxide catalysts for low temperature carbon monoxide oxidation. *Catal. Commun*., **2009**, *10*, 1776–1780.

[14] Chen, Y.; Zhang, Y.; Yao, Q.Z.; Zhou, G.T.; Fu, S.; Fan, H. Formation of α-Mn_2O_3 nanorods via a hydrothermal-assisted cleavage-decomposition mechanism. *J. Solid State Chem*., **2007**, *180*, 1218–1223.

[15] Ramarajan, D.; Sivagurunathan, P. Effects of surfactants on morphology in synthesis of α-Mn_2O_3 nanostructures. *J. Solid State Chem*., **2011**, *184*, 597–600.

[16] Liu, L.; Liang, H.; Yang, H.; Wei, J.; Yang, Y. The size-controlled synthesis of uniform Mn_2O_3 octahedra assembled from nanoparticles and their catalytic properties. *Nanotechnol*., **2011**, *22*, 015603 (8pp).

[17] Kunkalekar, R.K.; Salker, A.V. Low temperature carbon monoxide oxidation over nanosized silver doped manganese dioxide catalysts. *Catal. Commun*., **2010**, *12*, 193–196.

[18] Han, Y.F., Chen, L.; Ramesh, K.; Widjaja, E.; Chilukoti, S.; Surjami, I.K.; Chen, J. Kinetic and spectroscopic study of methane combustion over α-Mn_2O_3 nanocrystal catalysts. *J. Catal*., **2008**, *253*, 261–268.

[19] Hashem, A.M.A.; Mohamed, H.A.; Bahloul, A.; Eid, A.E.; Julien, C.M. Thermal stabilization of tin- and cobalt-doped manganese dioxide. *Ionics*, **2008**, *14*, 7–14.

[20] Kunkalekar, R.K.; Salker, A.V. Low temperature CO oxidation over nano-sized Cu–Pd doped MnO_2 catalysts. *Reac. Kinet. Mech. Cat*., **2013**, *108*, 173–182.

[21] Devaraj, S.; Munichandraiah, N. Effect of crystallographic structure of MnO_2 on its electrochemical capacitance properties. *J. Phys. Chem. C*, **2008**, *112*, 4406–4417.

[22] Julien, C.M.; Massot, M.; Poinsignon, C. Lattice vibrations of manganese oxides: Part I. Periodic structures. *Spectrochemica Acta A*, **2004**, *60*, 689–700.

[23] Shao, C.; Guan, H.; Liu, Y.; Li, X.; Yang, X. Preparation of Mn_2O_3 and Mn_3O_4 nanofibers via an electrospinning technique. *J. Solid State Chem*., **2004**, *177*, 2628–2631.

[24] Mars, P.; Van Krevelen, D.W. Oxidations carried out by means of vanadium oxide catalysts. *Chem. Eng. Sci. Spec. Suppl*., **1954**, *3*, 41–59.

Received: June 13, 2013 Revised: July 07, 2013 Accepted: July 15, 2013